ACS OMEGA

Open Access

http://pubs.acs.org/journal/acsodf

Article

Formation Process of $SiF_6@Cu_2L_4$ Chiral Cage Pairs in a Glass Vessel: Catechol Oxidation Catalysis and Chiral Recognition

Hyo Jeong Back, Daeun Kim, Dongwon Kim, Jihun Han, Mohammad Mozammal Hossain, Ok-Sang Jung,* and Young-A Lee*

Cite This: *ACS Omega* 2023, 8, 39720−39729

Read Online

ACCESS | Metrics & More | Article Recommendations | Supporting Information

ABSTRACT: Self-assembly of CuX_2 (X^- = BF_4^-, PF_6^-, and SbF_6^-) with a pair of chiral bidentate ligands, (1*R*,2*S*)-(+)- and (1*S*,2*R*)-(−)-1-(nicotinamido)-2,3-dihydro-1*H*-inden-2-yl-nicotinate (*r,s*-L or *s,r*-L), in a mixture solvent including ethanol in a glass vessel gives rise to SiF_6^{2-}-encapsulated Cu_2L_4 chiral cage products. The SiF_6^{2-} anion from the reaction of X^- with SiO_2 of the glass-vessel surface acts as a cage template or cage bridge. One of the products, $[SiF_6@Cu_2(SiF_6)(s,r\text{-L})_4]\cdot 3CHCl_3\cdot 4EtOH$, is one of the most effective heterogeneous catalysts for the oxidation of 3,5-di-*tert*-butylcatechol. Furthermore, an *l*-DOPA/*d*-DOPA pair is recognizable by the cyclic voltammetry (CV) signals of its combination with chiral cages $[SiF_6@Cu_2(BF_4)_2(s,r\text{- or } r,s\text{-L})_4]\cdot 4CHCl_3\cdot 2EtOH$ pair and $[SiF_6@Cu_2(SiF_6)(s,r\text{- or } r,s\text{-L})_4]\cdot 3CHCl_3\cdot 4EtOH$ pair.

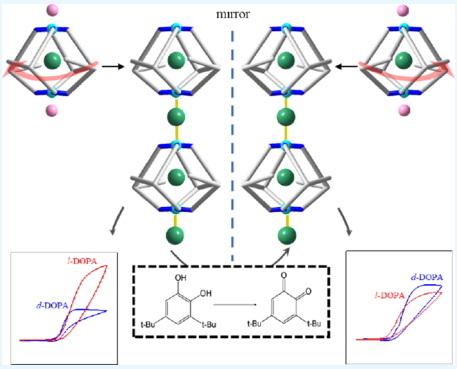

INTRODUCTION

Notable research results on chiral coordination cages for recognition of targeting chiral molecules have been reported since enantio-recognition became a subject of great interest in various chiral fields such as pharmaceuticals, pesticides, cosmetics, environmental pollutants, bioactive food products, and catalysis.[1−8] A number of different chiral coordination cages have been synthesized via a stereogenic center, atropisomerism, or noncovalent interactions for task-specific chiral applications.[9−14] Both the confined space and interaction site of chiral cage hosts are pivotal to the feasibility of chiral recognitions, and thus, such factors should be considered in constructing new chiral cages. In addition, (counter)anions significantly affect specific functions including catalysis of coordination cages, owing to a variety of features such as negative charge, size, geometry, solvent effects, and sensitive pH dependence.[15−23] Copper(II) catalysis oxidation of catechols into the corresponding *o*-quinones along with the reduction of oxygen to water[24] is an important process in the field of biomimetic oxidases.[25−27] Catechol oxidation catalysis using copper catalysts is sensitive to the nature of coligands, ligands, the Cu···Cu distance, electrochemical potentials, and pH change.[28−34] On the other hand, dihydroxyphenylalanine (DOPA) has been regarded as an important chiral molecule in the fields of medicine, biology, and marine adhesion.[35−38] *l*-DOPA, for instance, is known to play a crucial role at the clinical level and in neurochemistry with respect to Parkinson's disease, in contrast to its chiral isomer, inactive and toxic *d*-DOPA.[39,40] Previously, our group achieved enantioselective electrochemical recognition of various amino acids.[41−44] In this context, the central objective of the present study was efficient construction of a pair of chiral coordination cages, catechol oxidation, and enantio-recognition of *l*- and *d*-DOPA. Herein, we report chiral Cu_2L_4 cage pairs obtained by the self-assembly of CuX_2 with a newly designed pair of *s,r*- or *r,s*-chiral bidentate ligands. Chiral Cu_2L_4 cage pairs have been employed for enantio-recognition of chiral DOPA via a cyclic voltammetry (CV) technique.[45] The secondary aim of this study was to investigate the cage system's significant anion effects on catechol oxidation catalysis. To the best of our knowledge, the present stable 1D linked cages represent a landmark in the heterogeneous oxidation catalytic efficiency of catechol.

EXPERIMENTAL SECTION

Materials and Measurements. All of the chemicals including copper(II) tetrafluoroborate ($Cu(BF_4)_2$), copper(II) chloride ($CuCl_2$), silver(I) hexafluoroantimonate ($AgSbF_6$), and silver(I) hexafluorophosphate ($AgPF_6$) were purchased from Aldrich and used without further purification. Glass vessels (Hubena Co., Seongnam, Korea) were employed in all of the self-assembly reactions. The ^1H NMR spectra were

Received: August 2, 2023
Accepted: October 3, 2023
Published: October 13, 2023

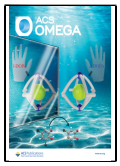

recorded on a Varian Mercury Plus 400 instrument operating at 400 MHz. The infrared (IR) spectra were obtained on a Nicolet 380 FT-IR spectrophotometer, with samples prepared as KBr pellets. Elemental microanalyses (C, H, and N) were performed on solid samples by the Pusan Center, KBSI, using a Vario-EL III. Thermal analyses were carried out under a dinitrogen atmosphere at a scan rate of 10 °C/min using a Labsys TGA-DSC 1600.

Synthesis of (1S,2R)-(−)-1-(Nicotinamido)-2,3-dihydro-1H-inden-2-yl Nicotinate (s,r-L). *N,N*-Diisopropylethylamine (7.5 mL, 42.0 mmol) was slowly added to a stirred mixture of (1*S*,2*R*)-(−)-*cis*-1-amino-2-indanol (0.45 g, 3 mmol) and nicotinoyl chloride hydrochloride (5.43 g, 30 mmol) in tetrahydrofuran (60.0 mL). The reaction mixture was then refluxed for 24 h. The resulting solution was washed with an aqueous $NaHCO_3$ solution several times. The tetrahydrofuran layer was dried over anhydrous magnesium sulfate for 1 h. Then, this solution was precipitated with excess hexane to obtain the white solid in 80.0% yield (Scheme 1). Anal. calcd

Scheme 1. Synthetic Procedure for *s,r*-L and *r,s*-L: *N,N*-Diisopropylethylamine, Tetrahydrofuran, N_2 at 80 °C for 24 h

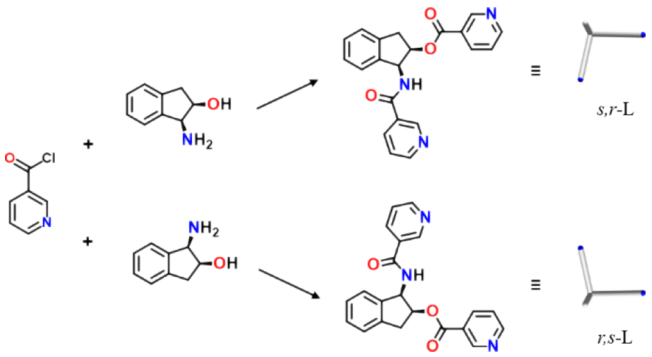

for $C_{21}H_{17}N_3O_3$: C, 70.18; H, 4.77; N, 11.69%. Found: C, 70.00; H, 4.47; N, 11.15%. IR (KBr pellet, cm^{-1}): 3290(m), 1722(s), 1638(s), 1590(m), 1542(m), 1482(w), 1423(w), 1350(w), 1290(m), 1200(w), 1124(m), 1025(m), 915(w), 744(m), 705(m), 627(w), 581(w), 510(w). ^1H NMR (dissociated in Me_2SO-d_6, δ): 8.35 (s, 1H), 8.27 (s, 1H), 8.15 (s, 1H), 7.96 (dd, J_1 = 4.75 Hz, J_2 = 1.63 Hz, 1H), 7.86 (dd, J_1 = 4.75 Hz, J_2 = 1.63 Hz, 1H), 7.46 (dt, J_1 = 7.88 Hz, J_2 = 1.88 Hz, 1H), 7.36 (dt, J_1 = 7.88 Hz, J_2 = 1.88 Hz, 1H), 6.69 (dd, J_1 = 7.50 Hz, J_2 = 4.88 Hz, 1H), 6.64 (dd, J_1 = 7.50 Hz, J_2 = 4.88 Hz, 1H), 6.60 (t, J_1 = 3.38 Hz, J_2 = 4.88 Hz, 1H), 6.56 (t, J_1 = 3.38 Hz, J_2 = 4.88 Hz, 1H), 6.53 (d, J_1 = 4.13 Hz, 1H), 6.51 (d, J_1 = 5.38 Hz, 1H), 5.07 (td, J_1 = 16.88 Hz, J_2 = 5.63 Hz, 1H), 5.03 (d, J = 5.63 Hz, 1H).

Synthesis of (1R,2S)-(+)-1-(Nicotinamido)-2,3-dihydro-1H-inden-2-yl Nicotinate (r,s-L). *N,N*-Diisopropylethylamine (7.5 mL, 42.0 mmol) was slowly added to a stirred mixture of (1*R*,2*S*)-(+)-cis-1-amino-2-indanol (0.45 g, 3 mmol) and nicotinoyl chloride hydrochloride (5.43 g, 30 mmol) in tetrahydrofuran (60.0 mL). The reaction mixture was then refluxed for 24 h. The resulting solution was washed with aqueous $NaHCO_3$ solution several times. The tetrahydrofuran layer was dried over anhydrous magnesium sulfate for 1 h. Then, this solution was precipitated by excess hexane to obtain a white solid in 78.0% yield. Anal. calcd for $C_{21}H_{17}N_3O_3$: C, 70.18; H, 4.77; N, 11.69%. Found: C, 69.10; H, 4.58; N, 11.02%. IR (KBr pellet, cm^{-1}): 3290(m), 1722(s), 1638(s), 1590(m), 1542(m), 1482(w), 1423(w), 1350(w), 1290(m), 1200(w), 1124(m), 1025(m), 915(w), 744(m), 705(m), 627(w), 581(w), 510(w). ^1H NMR (dissociated in Me_2SO-d_6, δ): 8.35 (s, 1H), 8.27 (s, 1H), 8.15 (s, 1H), 7.96 (dd, J_1 = 4.75 Hz, J_2 = 1.63 Hz, 1H), 7.86 (dd, J_1 = 4.75 Hz, J_2 = 1.63 Hz, 1H), 7.46 (dt, J_1 = 7.88 Hz, J_2 = 1.88 Hz, 1H), 7.36 (dt, J_1 = 7.88 Hz, J_2 = 1.88 Hz, 1H), 6.69 (dd, J_1= 7.50 Hz, J_2 = 4.88 Hz, 1H), 6.64 (dd, J_1 = 7.50 Hz, J_2 = 4.88 Hz, 1H), 6.60 (t, J_1 = 3.38 Hz, J_2 = 4.88 Hz, 1H), 6.56 (t, J_1 = 3.38 Hz, J_2 = 4.88 Hz, 1H), 6.53 (d, J_1 = 4.13 Hz, 1H), 6.51 (d, J_1 = 5.38 Hz, 1H), 5.07 (td, J_1 = 16.88 Hz, J_2 = 5.63 Hz, 1H), 5.03 (d, J = 5.63 Hz, 1H).

$[SiF_6@Cu_2(BF_4)_2(s,r\text{-}L)_4]\cdot 4CHCl_3\cdot 2EtOH$. An anhydrous ethanol solution (2.0 mL) of copper(II) tetrafluoroborate (2.35 mg, 0.01 mmol) was carefully layered onto a chloroform solution (1.0 mL) of *s,r*-L (3.59 mg, 0.01 mmol). After 5 days, blue crystals suitable for single-crystal X-ray crystallography were obtained in 84% yield. mp 223 °C (dec.). Anal. calcd for $C_{92}H_{84}B_2Cl_{12}Cu_2F_{14}N_{12}O_{14}Si$: C, 45.10; H, 3.46; N, 6.86%. Found: C, 45.00; H, 3.49; N, 6.70%. IR (KBr pellet, cm^{-1}): 3452(m), 3294(m), 1726(s), 1660(s), 1539(s), 1481(m), 1432(m), 1363(m), 1298(s), 1202(w), 1126(s), 1084(s), 1062(s), 1032(s), 913(w), 829(w), 745(s), 692(s), 651(m), 538(w), 520(w), 463(w).

$[SiF_6@Cu_2(BF_4)_2(r,s\text{-}L)_4]\cdot 4CHCl_3\cdot 2EtOH$. An anhydrous ethanol solution (2.0 mL) of copper(II) tetrafluoroborate (2.35 mg, 0.01 mmol) was carefully layered onto a chloroform solution (1.0 mL) of *r,s*-L (3.59 mg, 0.01 mmol). After 5 days, blue crystals suitable for single-crystal X-ray diffraction were obtained in 82% yield. mp 223 °C (dec.). Anal. calcd for $C_{92}H_{84}B_2Cl_{12}Cu_2F_{14}N_{12}O_{14}Si$: C, 45.10; H, 3.46; N, 6.86%. Found: C, 45.30; H, 3.38; N, 6.88%. IR (KBr pellet, cm^{-1}): 3452(m), 3294(m), 1726(s), 1660(s), 1539(s), 1481(m), 1432(m), 1363(m), 1298(s), 1202(w), 1126(s), 1084(s), 1062(s), 1032(s), 913(w), 829(w), 745(s), 692(s), 651(m), 538(w), 520(w), 463(w).

$[SiF_6@Cu_2(SiF_6)(s,r\text{-}L)_4]\cdot 3CHCl_3\cdot 4EtOH$. For method 1, an ethanol solution (2.0 mL) of copper(II) tetrafluoroborate (2.35 mg, 0.01 mmol) was carefully layered onto a chloroform solution (2.0 mL) of *s,r*-L (3.59 mg, 0.01 mmol). After 2 months, blue crystals suitable for single-crystal X-ray diffraction were obtained in 83% yield. For method 2, an ethanol solution (2.0 mL) of copper(II) tetrafluoroborate (2.35 mg, 0.01 mmol) was layered onto a chloroform solution (2.0 mL) of *s,r*-L (3.59 mg, 0.01 mmol), and then an aqueous solution (0.1 mL) of $(NH_4)_2SiF_6$ (3.60 mg, 0.02 mmol) was dropped into the solution. After 2 weeks, blue crystals suitable for single-crystal X-ray spectroscopy were obtained in a 75% yield. mp 232 °C (dec.). Anal. calcd for $C_{95}H_{95}Cl_9Cu_2F_{12}N_{12}O_{16}Si_2$: C, 47.72; H, 4.00; N, 7.03%. Found: C, 47.30; H, 4.09; N, 6.92%. IR (KBr pellet, cm^{-1}): 3452(m), 3294(m), 1726(s), 1660(s), 1539(s), 1481(m), 1423(w), 1350(w), 1290(m), 1200(w), 1124(m), 1025(m), 915(w), 829(w), 745(s), 692(s), 651(m), 538(w), 520(w), 463(w).

$[SiF_6@Cu_2(SiF_6)(r,s\text{-}L)_4]\cdot 3CHCl_3\cdot 4EtOH$. For method 1, an ethanol solution (2.0 mL) of copper(II) tetrafluoroborate (2.35 mg, 0.01 mmol) was carefully layered onto a chloroform solution (2.0 mL) of *r,s*-L (3.59 mg, 0.01 mmol). After 2 months, blue crystals suitable for single-crystal X-ray spectroscopy were obtained in 81% yield. For method 2, an ethanol solution (2.0 mL) of copper(II) tetrafluoroborate (2.35 mg, 0.01 mmol) was layered onto a chloroform solution (2.0 mL)

https://doi.org/10.1021/acsomega.3c05659
ACS Omega 2023, 8, 39720−39729

Table 1. Relevant Structural Data of Four Pairs of Chiral Cages

	$[SiF_6@Cu_2(BF_4)_2(s,r\text{-}L)_4]\cdot 4CHCl_3\cdot 2EtOH$	$[SiF_6@Cu_2(SiF_6)(s,r\text{-}L)_4]\cdot 3CHCl_3\cdot 4EtOH$	$[SiF_6@Cu_2(PF_6)_2(s,r\text{-}L)_4]\cdot 2CHCl_3\cdot 3EtOH$	$[SiF_6@Cu_2(SbF_6)_2(s,r\text{-}L)_4]\cdot 2CHCl_3\cdot 4EtOH$
Cu(1)···Cu(2)	7.893(3)	7.952(2)	7.8712(8)	7.8829(8)
Cu−F (outside anion)	2.5164(9), 2.341(7)	2.2689(5)	2.5986(3), 2.3553(2)	2.3091(2), 2.5087(3)
Cu−$FSiF_5$ (inside anion)	2.207(5), 2.288(6)	2.2490(5), 2.3453(5)	2.1866(2), 2.2924(2)	2.2544(2), 2.2215(2)
V (Å^3)	2673.7(2)	5979(2)	9127(3)	9533(3)
	$[SiF_6@Cu_2(BF_4)_2(r,s\text{-}L)_4]\cdot 4CHCl_3\cdot 2EtOH$	$[SiF_6@Cu_2(SiF_6)(r,s\text{-}L)_4]\cdot 3CHCl_3\cdot 4EtOH$	$[SiF_6@Cu_2(PF_6)_2(r,s\text{-}L)_4]\cdot 2CHCl_3\cdot 3EtOH$	$[SiF_6@Cu_2(SbF_6)_2(r,s\text{-}L)_4]\cdot 2CHCl_3\cdot 4EtOH$
Cu(1)···Cu(2)	7.926(3)	7.901(4)	7.890(1)	7.8573(8)
Cu−F (outside anion)	2.3358(9), 2.5599(9)	2.225(1)	2.3504(2), 2.5877(4)	2.5251(3), 2.2996(2)
Cu−$FSiF_5$ (inside anion)	2.2988(8), 2.2157(7)	2.212(1), 2.295(1)	2.280(4), 2.2113(3)	2.2338(2), 2.1962(2)
V (Å^3)	2716.3(1)	6061(7)	9313(3)	9466(3)

of *r,s*-L (3.59 mg, 0.01 mmol), and then an aqueous solution (0.1 mL) of $(NH_4)_2SiF_6$ (3.6 mg, 0.02 mmol) was dropped into the solution. After 2 weeks, blue crystals suitable for single-crystal X-ray crystallography were obtained in 74% yield. mp 232 °C (dec.). Anal. calcd for $C_{95}H_{95}Cl_9Cu_2F_{12}N_{12}O_{16}Si_2$: C, 47.72; H, 4.00; N, 7.03%. Found: C, 47.50; H, 3.97; N, 7.08%. IR (KBr pellet, cm^{-1}): 3452(m), 3294(m), 1726(s), 1660(s), 1539(s), 1481(m), 1423(w), 1350(w), 1290(m), 1200(w), 1124(m), 1025(m), 915(w), 829(w), 745(s), 692(s), 651(m), 538(w), 520(w), 463(w).

$[SiF_6@Cu_2(PF_6)_2(s,r\text{-}L)_4]\cdot 2CHCl_3\cdot 3EtOH$. An ethanol solution (2.0 mL) of silver(I) hexafluorophosphate (5.05 mg, 0.02 mmol) was added to copper(II) chloride (1.35 mg, 0.01 mmol) dispersed in ethanol at room temperature. The reaction mixture was stirred for 30 min, after which the precipitated silver chloride was filtered off. The ethanol solution of $Cu(PF_6)_2$ was carefully layered onto a chloroform solution (1.0 mL) of *s,r*-L (3.59 mg, 0.01 mmol). After 5 days, blue crystals suitable for X-ray single crystallography were obtained in 86% yield. mp 243 °C (dec.). Anal. calcd for $C_{92}H_{88}Cl_6Cu_2F_{18}N_{12}O_{15}P_2Si$: C, 46.55; H, 3.74; N, 7.08%. Found: C, 46.40; H, 3.70; N, 6.92%. IR (KBr pellet, cm^{-1}): 3443(m), 3307(m), 1733(s), 1663(s), 1539(s), 1481(m), 1435(m), 1358(m), 1298(s), 1204(w), 1133(s), 1058(w), 1030(w), 850(s), 745(s), 698(s), 651(m), 560(m), 428(w).

$[SiF_6@Cu_2(PF_6)_2(r,s\text{-}L)_4]\cdot 2CHCl_3\cdot 3EtOH$. An ethanol solution (2.0 mL) of silver(I) hexafluorophosphate (5.05 mg, 0.02 mmol) was added to copper(II) chloride (1.35 mg, 0.01 mmol) dispersed in ethanol at room temperature. The reaction mixture was stirred for 30 min, after which the precipitated silver chloride was filtered off. The ethanol solution of $Cu(PF_6)_2$ was carefully layered onto a chloroform solution (1.0 mL) of *r,s*-L (3.59 mg, 0.01 mmol). After 5 days, blue crystals suitable for single-crystal X-ray diffraction were obtained in 78% yield. mp 243 °C (dec.). Anal. calcd for $C_{92}H_{88}Cl_6Cu_2F_{18}N_{12}O_{15}P_2Si$: C, 46.55; H, 3.74; N, 7.08%. Found: C, 46.40; H, 3.70; N, 6.93%. IR (KBr pellet, cm^{-1}): 3443(m), 3307(m), 1733(s), 1663(s), 1539(s), 1481(m), 1435(m), 1358(m), 1298(s), 1204(w), 1133(s), 1058(w), 1030(w), 850(s), 745(s), 698(s), 651(m), 560(m), 428(w).

$[SiF_6@Cu_2(SbF_6)_2(s,r\text{-}L)_4]\cdot 2CHCl_3\cdot 4EtOH$. An ethanol solution (2.0 mL) of silver(I) hexafluoroantimonate (6.85 mg, 0.02 mmol) was added to copper(II) chloride (1.35 mg, 0.01 mmol) dispersed in ethanol at room temperature. The reaction mixture was stirred for 30 min, after which the precipitated silver chloride was filtered off. The ethanol solution of $Cu(SbF_6)_2$ was carefully layered onto a chloroform solution (1.0 mL) of *s,r*-L (3.59 mg, 0.01 mmol). After 5 days, blue crystals suitable for X-ray single crystallography were obtained in 77% yield. mp 241 °C (dec.). $C_{94}H_{94}Cl_6Cu_2F_{18}N_{12}O_{16}Sb_2Si$; C, 43.40; H, 3.64; N, 6.46%. Found: C, 43.10; H, 3.60; N, 6.30%. IR (KBr pellets, cm^{-1}): 3439(m), 3310(m), 1731(s), 1663(s), 1539(s), 1484(m), 1432(m), 1358(m), 1298(s), 1202(w), 1134(s), 1062(w), 1031(w), 912(w), 829(w), 745(s), 698(s), 659(s), 636(s), 446(w).

$[SiF_6@Cu_2(SbF_6)_2(r,s\text{-}L)_4]\cdot 2CHCl_3\cdot 4EtOH$. An ethanol solution (2.0 mL) of silver(I) hexafluoroantimonate (6.85 mg, 0.02 mmol) was added to copper(II) chloride (1.35 mg, 0.01 mmol) dispersed in ethanol at room temperature. The reaction mixture was stirred for 30 min, after which the precipitated silver chloride was filtered off. The ethanol solution of $Cu(SbF_6)_2$ was carefully layered onto a chloroform solution (1.0 mL) of *r,s*-L (3.59 mg, 0.01 mmol). After 5 days, blue crystals suitable for X-ray crystallography were obtained in 83% yield. mp 241 °C (dec.). $C_{94}H_{94}Cl_6Cu_2F_{18}N_{12}O_{16}Sb_2Si$; C, 43.40; H, 3.64; N, 6.46%. Found: C, 42.90; H, 3.59; N, 6.37%. IR (KBr pellet, cm^{-1}): 3439(m), 3310(m), 1731(s), 1663(s), 1539(s), 1484(m), 1432(m), 1358(m), 1298(s), 1202(w), 1134(s), 1062(w), 1031(w), 912(w), 829(w), 745(s), 698(s), 659(s), 636(s), 446(w).

Catechol Oxidation Catalysis. 3,5-Di-*tert*-butylcatechol (3,5-DBuCat) was employed as the substrate for the present catalytic oxidation reactions. The copper(II) catalysts (0.01 mmol) were treated with the substrate (0.1 mmol) in 10 mL of acetone at room temperature or at 40 °C under aerobic conditions. The catalytic yields were monitored with reference to the UV−vis spectra and ^{1}H NMR.

Voltammetry. A screen-printed carbon electrode (SPCE) composed of carbon as a working electrode, Ag/AgCl (sat. KCl) as a reference, and platinum as a counter electrode was used in an electrochemical analysis. As a pretreatment, the potential was cycled from −0.2 to +0.6 V in 0.1 M phosphate buffer solution (pH 7.4) to stabilize the SPCE electrode. To prepare the modified electrode, the chiral complexes $[SiF_6@Cu_2(BF_4)_2(s,r\text{-}L)_4]\cdot 4CHCl_3\cdot 2EtOH$, $[SiF_6@Cu_2(BF_4)_2(r,s\text{-}L)_4]\cdot 4CHCl_3\cdot 2EtOH$, $[SiF_6@Cu_2(SiF_6)(s,r\text{-}L)_4]\cdot 3CHCl_3\cdot 4EtOH$, and $[SiF_6@Cu_2(SiF_6)(r,s\text{-}L)_4]\cdot 3CHCl_3\cdot 4EtOH$ were dispersed in 0.1 M PBS solution by sonication for 4 h and drop-casted onto the SPCE. *l*- and *d*-DOPA were dissolved in 0.1 M PBS to prepare 10 mL of a 1.0 mM solution. The electrochemical measurement was performed with a potentiostat/galvanostat (Kosentech model KST-P1; Physiolab, S.

https://doi.org/10.1021/acsomega.3c05659
ACS Omega 2023, 8, 39720−39729

Scheme 2. Construction Procedure, Catalytic Effects, and DOPA Recognition of $SiF_6@Cu_2L_4$ Chiral Cage Pairs along with Voltammetric Signals of the Chiral Cage Pairs with *l*-DOPA (Red Line) and *d*-DOPA (Blue Line)

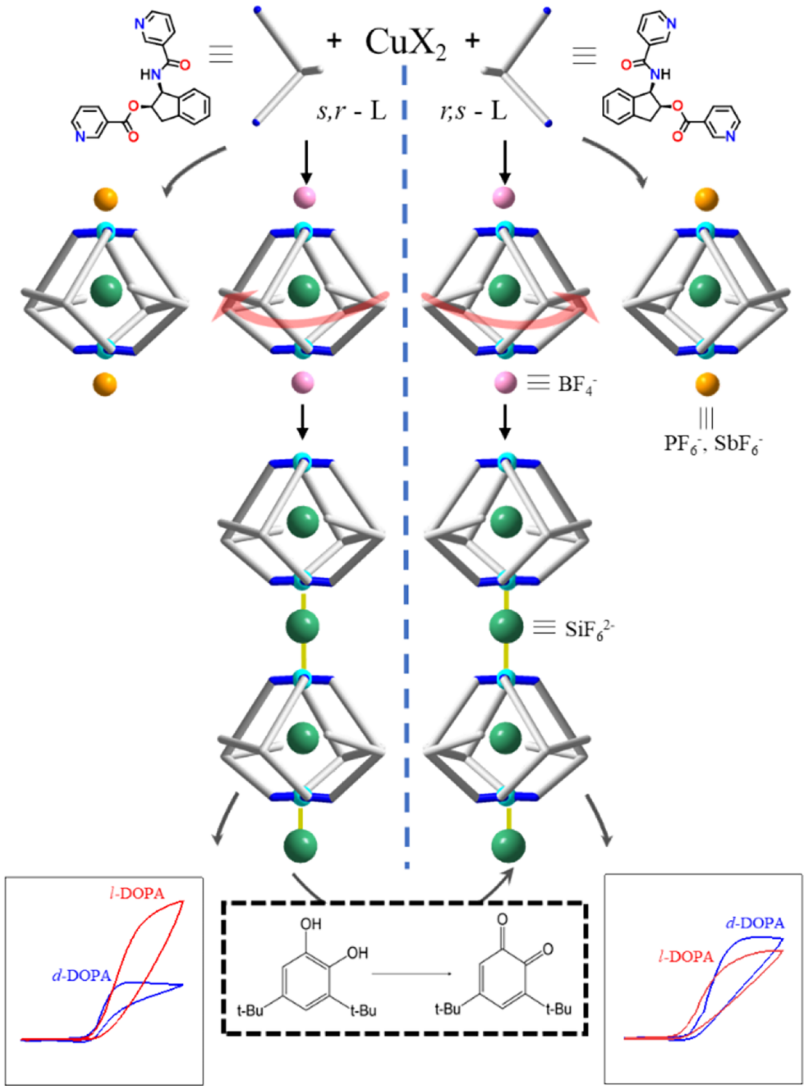

Korea). The cyclic voltammetry (CV) conditions were as follows: potential range, −0.2 to +0.6 V; scan rate, 100 mV/s; sensitivity, 10 μA.

Crystal Structure Determination. All of the X-ray diffraction data (except $[SiF_6@Cu_2(BF_4)_2(s,r\text{-}L)_4]\cdot 4CHCl_3\cdot 2EtOH$ and $[SiF_6@Cu_2(SiF_6)(r,s\text{-}L)_4]\cdot 3CHCl_3\cdot 4EtOH$) were measured at 223 K with synchrotron radiation (λ = 0.63000−0.70000 Å) on a Rayonix MX225HS detector at 2D SMC with a silicon (111) double-crystal monochromator (DCM) at the Pohang Accelerator Laboratory, Korea (Table 1). The PAL BL2D-SMDC program[46] was used for data collection (detector distance: 66 mm; omega scan: $\Delta\omega$ = 3°; exposure time: 1 s/frame), and HKL3000sm (ver. 703r)[47] was used for cell refinement, reduction, and absorption correction. X-ray data on $[SiF_6@Cu_2(BF_4)_2(s,r\text{-}L)_4]\cdot 4CHCl_3\cdot 2EtOH$ and $[SiF_6@Cu_2(SiF_6)(r,s\text{-}L)_4]\cdot 3CHCl_3\cdot 4EtOH$ were collected on a Bruker SMART automatic diffractometer with graphite-monochromated Mo Kα radiation (λ = 0.71073 Å). Thirty-six (36) frames of 2D diffraction images were collected and processed to obtain the cell parameters and orientation matrix. The data were corrected for Lorentz and polarization effects. The absorption effects were corrected using the multiscan method (SADABS).[48] The structures were solved using the direct method (SHELXS) and refined by a full-matrix least-squares technique (SHELXL 2018/3).[49] The nonhydrogen atoms were refined anisotropically, and the hydrogen atoms were placed in calculated positions and refined only for the isotropic thermal factors. The crystal parameters and procedural information corresponding to the data collection and structure refinement are listed in Table S1.

RESULTS AND DISCUSSION

Synthesis. Self-assembly of $Cu(BF_4)_2$ with a pair of chiral ligands in a mixture of ethanol and chloroform in a glass vessel produced, after 5 days, crystals consisting of a $[SiF_6@Cu_2(BF_4)_2(s,r\text{-}$ or $r,s\text{-}L)_4]\cdot 4CHCl_3\cdot 2EtOH$ pair suitable for single X-ray crystallography (Scheme 2). Subsequently, after a prolonged time (i.e., 2 months), the self-assembly in the mixture solvent gave rise to a $[SiF_6@Cu_2(SiF_6)(s,r\text{-}$ or $r,s\text{-}L)_4]\cdot 3CHCl_3\cdot 4EtOH$ pair. The self-assembly reactions of $Cu(PF_6)_2$ and $Cu(SbF_6)_2$ instead of $Cu(BF_4)_2$ with *s,r*- or *r,s*-L gave rise to $[SiF_6@Cu_2(PF_6)_2(s,r\text{-}$ or $r,s\text{-}L)_4]\cdot 2CHCl_3\cdot 3EtOH$ and $[SiF_6@Cu_2(SbF_6)_2(s,r\text{-}$ or $r,s\text{-}L)_4]\cdot 2CHCl_3\cdot 4EtOH$ after 5 days, respectively. $Cu(PF_6)_2$ and $Cu(SbF_6)_2$, in contrast to

https://doi.org/10.1021/acsomega.3c05659
ACS Omega 2023, 8, 39720−39729

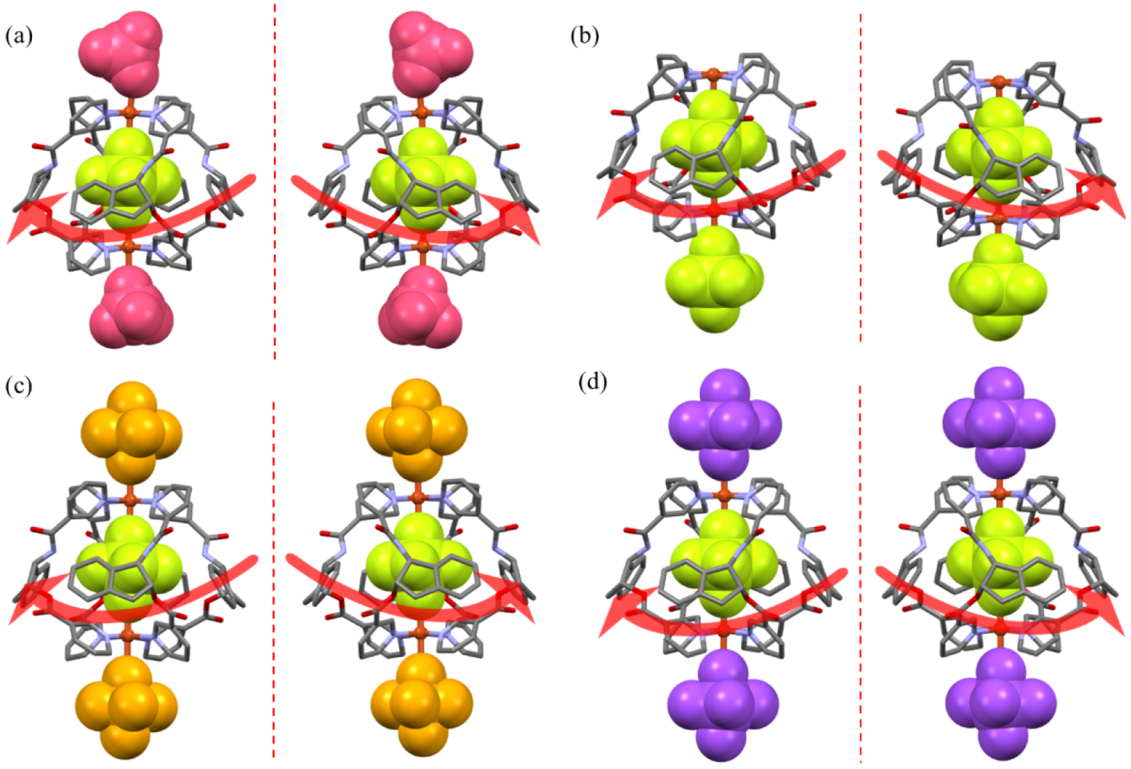

Figure 1. Crystal structures of pairs of chiral cages, $[SiF_6@Cu_2(BF_4)_2(s,r\text{-}L)_4]\cdot 4CHCl_3\cdot 2EtOH$ (left) and $[SiF_6@Cu_2(BF_4)_2(r,s\text{-}L)_4]\cdot 4CHCl_3\cdot 2EtOH$ (right) (a), $[SiF_6@Cu_2(SiF_6)(s,r\text{-}L)_4]\cdot 3CHCl_3\cdot 4EtOH$ (left) and $[SiF_6@Cu_2(SiF_6)(r,s\text{-}L)_4]\cdot 3CHCl_3\cdot 4EtOH$ (right) (b), $[SiF_6@Cu_2(PF_6)_2(s,r\text{-}L)_4]\cdot 2CHCl_3\cdot 3EtOH$ (left) and $[SiF_6@Cu_2(PF_6)_2(r,s\text{-}L)_4]\cdot 2CHCl_3\cdot 3EtOH$ (right) (c), and $[SiF_6@Cu_2(SbF_6)_2(s,r\text{-}L)_4]\cdot 2CHCl_3\cdot 4EtOH$ (left) and $[SiF_6@Cu_2(SbF_6)_2(r,s\text{-}L)_4]\cdot 2CHCl_3\cdot 4EtOH$ (right) (d).

$Cu(BF_4)_2$, did not yield $[SiF_6@Cu_2(SiF_6)(s,r\text{- or }r,s\text{-}L)_4]$ even after 2 months, indicating that the F-containing anion is a significant factor in anion transformation in a glass vessel, which had already clearly been reported by our laboratory.[50] For all reactions, the SiF_6^{2-} anion acts as a template to form products or a bridge between a cage and another cage. All products are Cu_2L_4 chiral coordination cage pairs containing an encapsulated SiF_6^{2-} from the reaction of F-containing polyatomic anions with the SiO_2 of the glass-vessel surface. That is, the anion, SiF_6^{2-}, is necessary as a template for the construction of the Cu_2L_4 cage. The Cu_2L_4 cage's formation of 1:2 composition was attributed to the intrinsic properties of the self-assembly condition. Not surprisingly then, it was found that the combination of the curved bidentate L conformer and the octahedral Cu(II) geometry, along with the nestled template, SiF_6^{2-}, might be a key driving force behind the formation of the Cu_2L_4 cage. Furthermore, their molecular dimensions are dependent on intercage interactions via outside anions, resulting in formation of either a 1D or discrete cage. That is, the metallophilicity of divalent SiF_6^{2-} as a bridge is stronger than that of the other monovalent counteranions, BF_4^-, PF_6^-, and SbF_6^-.[33] To confirm the different nature of the encapsulated anion and the outside anions, anion exchange was carried out.[33,50] Anion exchange of $[SiF_6@Cu_2(SbF_6)_2(s,r\text{- or }r,s\text{-}L)_4]\cdot 2CHCl_3\cdot 4EtOH$ with excess $NaPF_6$ in the ethanol suspension state resulted in an outside anion-exchanged species, $[SiF_6@Cu_2(PF_6)_2(s,r\text{- or }r,s\text{-}L)_4]\cdot 2CHCl_3\cdot 4EtOH$ (Figure S1). For construction of the coordination cage architecture, transformation of a specific anion as a template is a specific methodology for tuning the shape and topology of coordination species. The transformation of ubiquitous anions is worthy of insight, including their role. Encapsulated and bridged SiF_6^{2-} anions help to maintain the structure of cages.

All crystalline products are stable under aerobic conditions and are insoluble in common organic solvents such as chloroform, toluene, benzene, and tetrahydrofuran. They are partially dissociated in dimethyl sulfoxide and *N*,*N*-dimethylformamide. Their compositions and structures were confirmed in the current study by elemental analyses, ^1H NMR, circular dichroism, IR, TGA, EDS (Figures S2−S6), and single-crystal X-ray single crystallography. The characteristic IR bands of SiF_6^{2-} (696−755 cm^{-1}) were clearly assigned. TGA showed that they are stable up to 223−243 °C. Evaporation of the solvate molecules of the two kinds of crystals was found to occur in the 30−200 °C temperature range (Figure S5).

Crystal Structures. These pairs of Cu_2L_4 chiral cage crystals are classified into two categories: 1D and discrete species, depending on the outside anions. The crystal structure of $[SiF_6@Cu_2(BF_4)_2(s,r\text{-}L)_4]\cdot 4CHCl_3\cdot 2EtOH$ is a discrete cage, as depicted in Figure 1, and its bond lengths and angles are listed in Table S2. The geometry of each copper(II) ion is an octahedral N_4F_2 coordination arrangement with four N donors from four L's and two F donors from one SiF_6^{2-} and one BF_4^-anion (Cu−N = 1.979(9)−2.029(8) Å; Cu−F (SiF_6^{2-}) = 2.207(5) and 2.288(6) Å; Cu−F (BF_4^-) = 2.5164(9) and 2.341(7) Å) in axial positions, resulting in the formation of the Cu_2L_4 cage occupied by one SiF_6^{2-} anion. Concomitantly, for the nestled SiF_6^{2-} anion, the axial Si−F lengths (1.698(6) and 1.702(6) Å) are slightly longer than the equatorial Si−F bond lengths (1.653(7)−1.680(7) Å), owing to the axial Cu−F (SiF_6^{2-}) interactions. The intracage Cu···Cu distance is 7.893(3) Å. Two BF_4^- anions are coordinated to

https://doi.org/10.1021/acsomega.3c05659
ACS Omega 2023, 8, 39720−39729

two Cu(II) cations outside of the cage. The cages are packed in an eclipsed manner. The chloroform and ethanol molecules fill the empty space as a solvate without any significant interactions. The crystal structure of its enantiomer, $[SiF_6@Cu_2(BF_4)_2(r,s\text{-}L)_4]\cdot 4CHCl_3\cdot 2EtOH$, is an exact mirror image, as depicted in Figure 1 and Figure S7. The crystal structures of the $[SiF_6@Cu_2(PF_6)_2(s,r\text{- or }r,s\text{-}L)_4]\cdot 2CHCl_3\cdot 3EtOH$ and $[SiF_6@Cu_2(SbF_6)_2(s,r\text{- or }r,s\text{-}L)_4]\cdot 2CHCl_3\cdot 4EtOH$ pairs (Figure 1c,d) are very similar to those of the $[SiF_6@Cu_2(BF_4)_2(s,r\text{- or }r,s\text{-}L)_4]\cdot 4CHCl_3\cdot 2EtOH$ pair.

The crystal structure of $[SiF_6@Cu_2(SiF_6)(s,r\text{-}L)_4]\cdot 3CHCl_3\cdot 4EtOH$ is a 1D cage chain bridged by SiF_6^{2-}, as shown in Figure 2. There are two cages in an asymmetric unit. The local

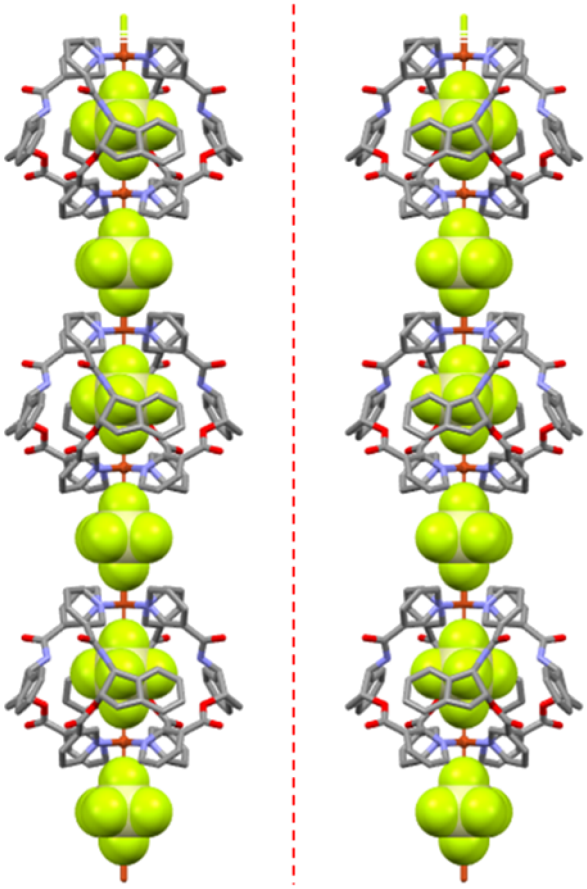

Figure 2. 1D linked cage structures for pairs of chiral cages, $[SiF_6@Cu_2(SiF_6)(s,r\text{-}L)_4]\cdot 3CHCl_3\cdot 4EtOH$ (left) and $[SiF_6@Cu_2(SiF_6)(r,s\text{-}L)_4]\cdot 3CHCl_3\cdot 4EtOH$ (right).

geometry of the Cu(II) ion is an octahedral arrangement with two SiF_6^{2-} groups in the *trans* position (Cu−F = 2.2574(5) and 2.2490(5) Å; F−Cu−F′ = 180.0°) and four pyridine N donors of four L's on the basal plane. Each L connects two Cu(II) ions in a bridged-bidentate mode to form the cage. The intracage Cu(II)···Cu(II) distances are 7.952(2) Å. Its packing structure is in the linear mode of cage···SiF_6^{2-}···cage···SiF_6^{2-} via electrostatic interactions (Cu···$FSiF_5$ = 2.2490(5) and 2.2689(5) Å), resulting in the formation of 1D chains. The electrostatic interaction of the intercage Cu···SiF_6^{2-} is comparable to that of the intracage Cu···SiF_6^{2-}, indicating that the outside SiF_6^{2-} acts as a bridge rather than a simple counteranion. The solvate molecules are squeezed. The crystal structure of $[SiF_6@Cu_2(SiF_6)(r,s\text{-}L)_4]\cdot 3CHCl_3\cdot 4EtOH$ is a mirror image of $[SiF_6@Cu_2(SiF_6)(s,r\text{-}L)_4]\cdot 3CHCl_3\cdot 4EtOH$.

Catalysis of Catechol Oxidation. To test the catalytic activity of the Cu(II) cage species, 3,5-di-*tert*-butylcatechol (3,5-DBCat) was employed as the substrate for catalytic oxidation. The oxidized species, 3,5-di-*tert*-butyl-1,2-benzoquinone, is an important ligand for M-to-L electron transfer, exhibiting a strong absorption band at around 400 nm that can easily monitor the catalysis procedure.[30,33,34] The catalyses using a series of catalysts were carried out to scrutinize the outside anion effects of the cages. Each cage catalyst was treated with 3,5-DBCat in the 1:10 mol ratio under aerobic conditions in 10 mL of acetone at 40 °C.

Thus, the catalysis rates were checked with reference to the increase in the characteristic UV band at around 400 nm as a function of time (Figure 3), together with the ^{1}H NMR data (Figure 4).

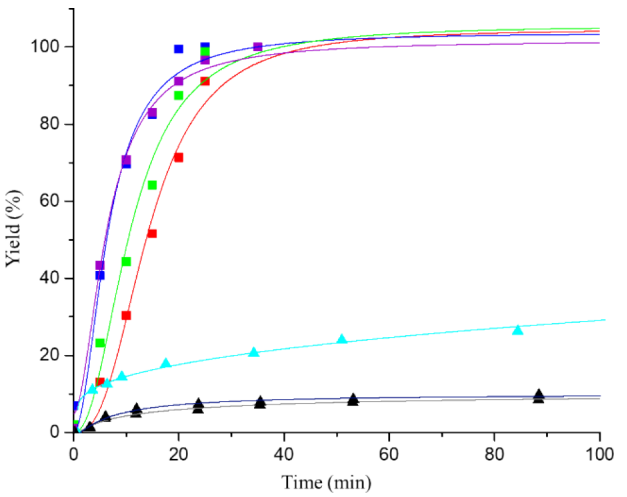

Figure 3. Catalytic oxidation rates of 3,5-di*tert*-butylcatechol using $[SiF_6@Cu_2(BF_4)_2(s,r\text{-}L)_4]\cdot 4CHCl_3\cdot 2EtOH$ (red solid square), $[SiF_6@Cu_2(SiF_6)(s,r\text{-}L)_4]\cdot 3CHCl_3\cdot 4EtOH$ (purple solid square), $[SiF_6@Cu_2(PF_6)_2(s,r\text{-}L)_4]\cdot 2CHCl_3\cdot 3EtOH$ (green solid square), $[SiF_6@Cu_2(SbF_6)_2(s,r\text{-}L)_4]\cdot 2CHCl_3\cdot 4EtOH$ (blue solid square), $Cu(BF_4)_2$ (cyan up-pointing solid triangle), $Cu(PF_6)_2$ (black up-pointing solid triangle), and $Cu(SbF_6)_2$ (gray up-pointing solid triangle).

All of the catalysis reactions were completely finished within 30 min, and the most remarkable feature was a solubility difference between two kinds of species: the discrete cages act as a homogeneous catalyst in acetone media, but the 1D chains act as a heterogeneous catalyst in acetone. The enhanced oxidation catalytic efficiency of the 1D and discrete cage catalysts is related to the maintenance of the intracage Cu···Cu distances (7.8573(8)−7.952(2) Å), which is suitable for coordination with the catechol substrate,[33,51] indicating that the cage skeleton is maintained in both the solution and solid states. The efficiency in homogeneous catalysis of three discrete cages, $[SiF_6@Cu_2(BF_4)_2(s,r\text{-}L)_4]\cdot 4CHCl_3\cdot 2EtOH$, $[SiF_6@Cu_2(PF_6)_2(s,r\text{-}L)_4]\cdot 2CHCl_3\cdot 3EtOH$, and $[SiF_6@Cu_2(SbF_6)_2(s,r\text{-}L)_4]\cdot 2CHCl_3\cdot 4EtOH$, is not significantly different. A remarkable feature is that, uncommonly, heterogeneous catalysis is very efficient: the oxidation catalysis using the 1D chains is completely finished within 25 min. The efficiency of the 1D heterogeneous catalyst was more notable in the present study than that of the common catalytic systems. Heterogeneous catalysis using $[SiF_6@Cu_2(SiF_6)(s,r\text{-}L)_4]\cdot 3CHCl_3\cdot$

https://doi.org/10.1021/acsomega.3c05659
ACS Omega 2023, 8, 39720−39729

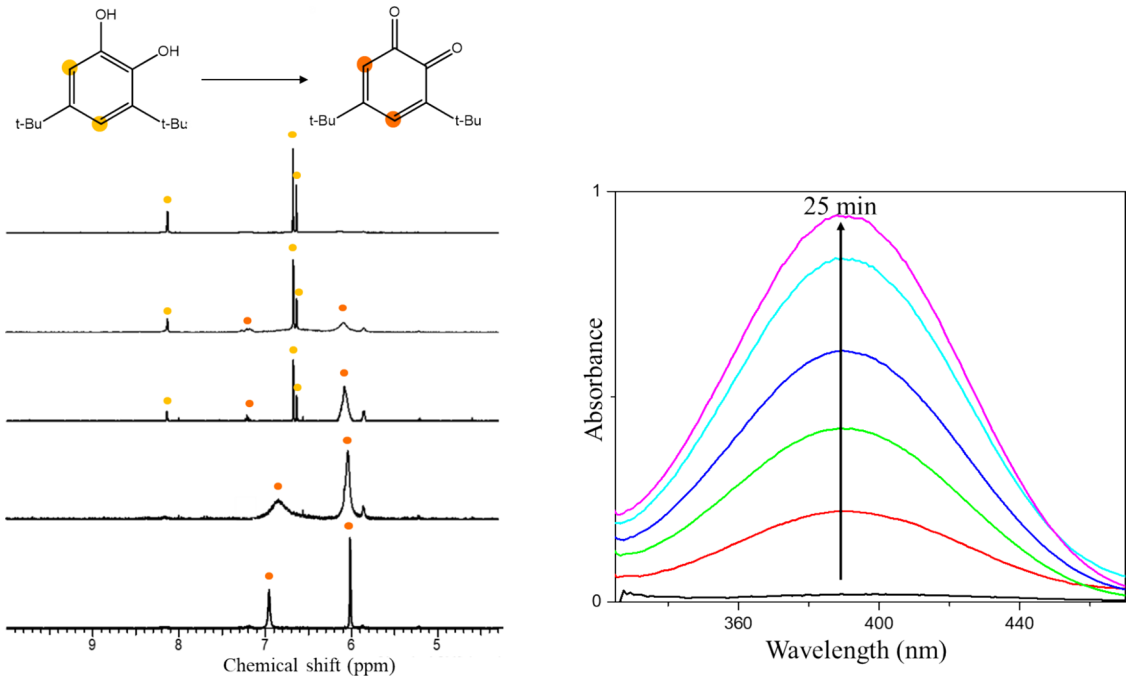

Figure 4. ^{1}H NMR spectral procedure on catalytic oxidation of 3,5-di-*tert*-butylcatechol to 3,5-di-*tert*-butylorthoquinone using $[SiF_6@Cu_2(SiF_6)(s,r\text{-}L)_4]\cdot 3CHCl_3\cdot 4EtOH$ in Me_2CO-d_6 (left). UV spectral change during the catalytic reaction (right).

4EtOH was the focus in this study. In particular, heterogeneous catalysis showed similar catalytic efficiency even at room temperature (Figure 5a). The solvent quantity may be another factor in heterogeneous catalysis, but for this catalysis, the efficiency in 10 mL of acetone was the same as that in 20 mL of acetone (Figure 5b), indicating that the catalyst is insoluble irrespective of the quantity of acetone. Further, after the catalysis was finished, the mixture solution was centrifuged to recover the broken crystalline catalyst. The IR, ^{1}H NMR spectra, and PXRD patterns indicated that the catalyst maintained the cage structure after the heterogeneous catalytic reaction (Figures S8 and S9). After the first heterogeneous catalytic reaction, a maximum of 90% of the catalyst could be recovered. The catalytic efficiency, moreover, was found to be perfectly recyclable (Figure 5c). Heterogeneous catalytic reactions according to various catalyst quantities (0.01, 0.005, 0.0025, and 0.00125 mmol for 0.1 mol of catechol) were carried out, and the catalytic rate depending on the decrease of the catalyst is gradually slow (Figure 5d).

Enantio-Recognition via CV. To estimate the chiral recognition abilities of one pair of the present chiral cages, *l*- and *d*-DOPA were employed as substrates to confirm the different interactions of each chiral cage with chiral DOPA via cyclic voltammetry (CV). The CV curves were measured in 0.1 M phosphate buffer solution (PBS, pH = 7.4) (Figure 6 and Figure S10). First of all, the oxidation peak of $[SiF_6@Cu_2(BF_4)_2(s,r\text{-}L)_4]\cdot 4CHCl_3\cdot 2EtOH$ in the solution including 1.0 mM *l*- and *d*-DOPA was observed at 350 and 270 mV, respectively. By contrast, the oxidation peaks of $[SiF_6@Cu_2(BF_4)_2(r,s\text{-}L)_4]\cdot 4CHCl_3\cdot 2EtOH$ with *l*-DOPA and *d*-DOPA were observed at 238 and 295 mV, respectively. Similarly, the oxidation peak of $[SiF_6@Cu_2(SiF_6)(s,r\text{-}L)_4]\cdot 3CHCl_3\cdot 4EtOH$ with *l*- and *d*-DOPA was observed at 405 and 275 mV, respectively, whereas that of $[SiF_6@Cu_2(SiF_6)(r,s\text{-}L)_4]\cdot 3CHCl_3\cdot 4EtOH$ with *l*-DOPA and *d*-DOPA was observed at 315 and 385 mV, respectively. These oxidation peaks indicate that the chiral cage interacts with oxidized chiral DOPA quinone.[52] That is, $[SiF_6@Cu_2(BF_4)_2(s,r\text{-}L)_4]\cdot 4CHCl_3\cdot 2EtOH$ interacts more strongly with *l*-DOPA, whereas $[SiF_6@Cu_2(BF_4)_2(r,s\text{-}L)_4]\cdot 4CHCl_3\cdot 2EtOH$ efficiently interacts with *d*-DOPA, resulting in higher oxidation potentials. Such a chiral cage system pair, therefore, can be used to differentiate the chirality of chiral DOPA. Thus, too, it can be applied for tailored storage or recognition of chiral molecules. Each chiral cage seems to contribute to the chiral recognition via the felicitous weak noncovalent interaction between a chiral cage and a chiral DOPA. This unique chiral cage system, therefore, can be extended for use as a system for recognition of the chiralities of general amino acids.

CONCLUSIONS

The new pair of bidentate chiral ligands is a valuable material for construction of Cu_2L_4 cage species via a template anion from transformation of polyatomic anions BF_4^-, PF_6^-, and SbF_6^- into SiF_6^{2-} during self-assembly in a glass vessel. The molecular dimensions of the cages are dependent on the metallophilicity of the outside anions. This series of Cu(II) cages is a good model system that shows significant oxidation catalytic effects on both the cage structure and solubility. The most attractive feature is the effectiveness of heterogeneous catalysis, including its recyclability, which indicates that the retained molecular structure plays a key role in the catalysis. In particular, a pair of chiral cages is a very useful molecular material for recognition of chiral substrates via electrochemical techniques. The present pair of chiral cages can be considered to be a highly useful molecular system for the recognition of targeting chiral molecules. Further experiments on chiral cage system pairs, including the electronic and steric effects of new silicon-containing ligands, will provide for wider and more practical applications of the enormous potential of the cages' catalytic properties and various chiral recognition functions.

https://doi.org/10.1021/acsomega.3c05659
ACS Omega 2023, 8, 39720−39729

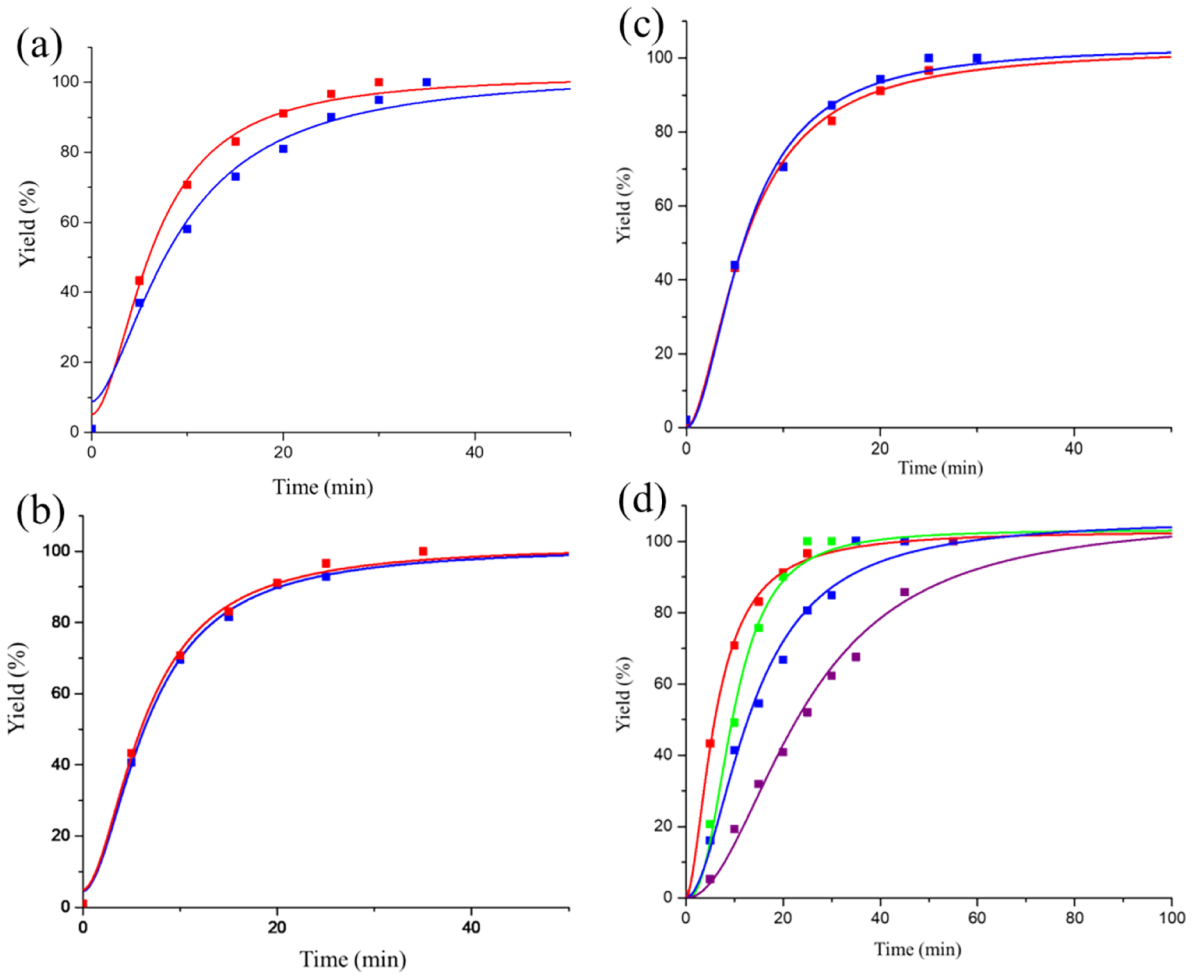

Figure 5. Catalytic oxidation rates of 3,5-di-*tert*-butylcatechol using $[SiF_6@Cu_2(SiF_6)(s,r\text{-}L)_4]\cdot 3CHCl_3\cdot 4EtOH$ in acetone at 40 °C (red line) and at room temperature (blue line) (a) and in 10 mL of acetone (red line) and in 20 mL of acetone (blue line) (b) and $[SiF_6@Cu_2(SiF_6)(s,r\text{-}L)_4]\cdot 3CHCl_3\cdot 4EtOH$ in acetone (red line) and recycled catalyst (blue line) in acetone (c) and depending on catalyst quantity, 0.01 (red line), 0.005 (green line), 0.0025 (blue line), and 0.00125 mmol (purple line) for 0.1 mmol of catechol (d).

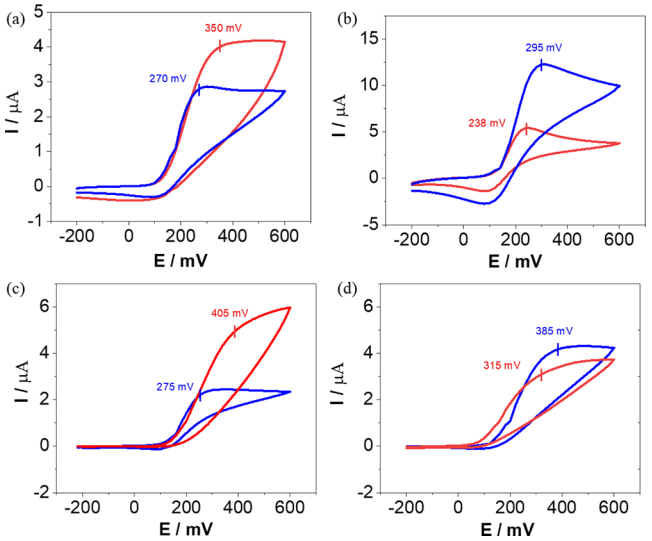

Figure 6. Cyclic voltammetry (CV) signals of $[SiF_6@Cu_2(BF_4)_2(s,r\text{-}L)_4]\cdot 4CHCl_3\cdot 2EtOH$ (a), $[SiF_6@Cu_2(BF_4)_2(r,s\text{-}L)_4]\cdot 4CHCl_3\cdot 2EtOH$ (b), $[SiF_6@Cu_2(SiF_6)(s,r\text{-}L)_4]\cdot 3CHCl_3\cdot 4EtOH$ (c), and $[SiF_6@Cu_2(SiF_6)(r,s\text{-}L)_4]\cdot 3CHCl_3\cdot 4EtOH$ (d) in the presence of 1.0 mM *l*-DOPA (red line) and *d*-DOPA (blue line).

■ ASSOCIATED CONTENT

Supporting Information

The Supporting Information is available free of charge at https://pubs.acs.org/doi/10.1021/acsomega.3c05659.

Experimental details including IR spectra, TG curves, CV signals, and ^{1}H NMR spectra (PDF)

Accession Codes

CCDC 2285883−2285890 contain the supplementary crystallographic data for this paper. These data can be obtained free of charge at www.ccdc.cam.ac.uk/data_request/cif, or by emailing to data_request@ccdc.cam.ac.uk, or by contacting The Cambridge Crystallographic Data Centre, 12 Union Road, Cambridge CB2 1EZ, UK; fax: + 44 1223 336033.

■ AUTHOR INFORMATION

Corresponding Authors

Ok-Sang Jung − *Department of Chemistry, Pusan National University, Busan 46241, Republic of Korea;* orcid.org/0000-0002-7218-457X; Phone: +82-51-510-2591; Email: oksjung@pusan.ac.kr; Fax: +83-52-516-7421

Young-A Lee − *Department of Chemistry, Jeonbuk National University, Jeonju 54896, Republic of Korea*; Phone: +82-63-270-33347; Email: ylee@jbnu.ac.kr

https://doi.org/10.1021/acsomega.3c05659
ACS Omega 2023, 8, 39720−39729

Authors

Hyo Jeong Back − *Department of Chemistry, Pusan National University, Busan 46241, Republic of Korea*

Daeun Kim − *Department of Chemistry, Pusan National University, Busan 46241, Republic of Korea*

Dongwon Kim − *Department of Chemistry, Pusan National University, Busan 46241, Republic of Korea;* orcid.org/0000-0002-7950-5487

Jihun Han − *Department of Chemistry, Pusan National University, Busan 46241, Republic of Korea*

Mohammad Mozammal Hossain − *Department of Electrochemistry, Korea Institute of Materials Science (KIMS), Changwon 51508, Republic of Korea*

Complete contact information is available at: https://pubs.acs.org/10.1021/acsomega.3c05659

Notes

The authors declare no competing financial interest.

■ ACKNOWLEDGMENTS

This work was supported by National Research Foundation of Korea (NRF) grants funded by the Korean Government [MEST] (2021R1A2C2005105 (OSJ) and 2021R1I1A3059982 (YAL)). The X-ray crystallography at the PLS-II 2D-SMC beamline was supported in part by MSIP and POSTECH.

■ REFERENCES

(1) Li, X.; Wu, J.; He, C.; Meng, Q.; Duan, C. Asymmetric catalysis within the chiral confined space of metal−organic architectures. *Small* **2019**, *15* (32), No. 1804770.

(2) Ronson, T. K.; Carpenter, J. P.; Nitschke, J. R. Dynamic optimization of guest binding in a library of diastereomeric heteroleptic coordination cages. *Chem.* **2022**, *8* (2), 557−568.

(3) Jung, M. J.; Paladhi, S.; Song, C. E. Enantioselective protonation of monofluorinated silyl enol ethers by cooperative cation-binding catalysis. *Bull. Korean Chem. Soc.* **2023**, *44* (5), 420−424.

(4) Brzechwa-Chodzyńska, A.; Drożdż, W.; Harrowfield, J.; Stefankiewicz, A. R. Fluorescent sensors: A bright future for cages. *Coord. Chem. Rev.* **2021**, *434*, No. 213820.

(5) Ribeiro, C.; Ribeiro, A. R.; Maia, A. S.; Tiritan, M. E. Occurrence of chiral bioactive compounds in the aquatic environment: a review. *Symmetry* **2017**, *9* (10), 215.

(6) He, Y.-P.; Yuan, L.-B.; Song, J.-S.; Chen, G.-H.; Lin, Q.; Li, C.; Zhang, L.; Zhang, J. Optical resolution of the water-soluble $Ti_4(embonate)_6$ cages for enantioselective recognition of chiral drugs. *Chem. Mater.* **2018**, *30* (21), 7769−7775.

(7) Li, X.; Ma, Q.; Zheng, X.; Chen, Q.; Sun, X. Recent applications and chiral separation developments based on stationary phases in open tubular capillary electrochromatography (2019−2022). *J. Pharm. Anal.* **2023**, *13* (4), 323−339.

(8) Bao, S.; Wu, S.; Huang, L.; Xu, X.; Xu, R.; Li, Y.; Liang, Y.; Yang, M.; Yoon, D. K.; Lee, M. Supramolecular nanopumps with chiral recognition for moving organic pollutants from water. *ACS Appl. Mater. Interfaces* **2019**, *11* (34), 31220−31226.

(9) Schulte, T. R.; Holstein, J. J.; Clever, G. H. Chiral self-discrimination and guest recognition in helicene-based coordination cages. *Angew. Chem., Int. Ed.* **2019**, *58* (17), 5562−5566.

(10) Wu, K.; Tessarolo, J.; Baksi, A.; Clever, G. H. Guest-modulated circularly polarized luminescence by ligand-to-ligand chirality transfer in heteroleptic Pd^{II} coordination cages. *Angew. Chem., Int. Ed.* **2022**, *61* (35), No. e202205725.

(11) Zhang, D.; Ronson, T. K.; Zou, Y.-Q.; Nitschke, J. R. Metal−organic cages for molecular separations. *Nat. Rev. Chem.* **2021**, *5* (3), 168−182.

(12) Guo, J.; Xu, Y. W.; Li, K.; Xiao, L. M.; Chen, S.; Wu, K.; Chen, X. D.; Fan, Y. Z.; Liu, J. M.; Su, C. Y. Regio-and enantioselective photodimerization within the confined space of a homochiral ruthenium/palladium heterometallic coordination cage. *Angew. Chem., Int. Ed.* **2017**, *56* (14), 3852−3856.

(13) Howlader, P.; Zangrando, E.; Mukherjee, P. S. Self-assembly of enantiopure Pd_{12} tetrahedral homochiral nanocages with tetrazole linkers and chiral recognition. *J. Am. Chem. Soc.* **2020**, *142* (19), 9070−9078.

(14) Grajda, M.; Staros, G.; Jędrzejewska, H.; Szumna, A. Toward coordination cages with hybrid chirality: amino acid-induced chirality on metal centers. *Inorg. Chem.* **2022**, *61* (29), 11410−11418.

(15) Rancan, M.; Tessarolo, J.; Carlotto, A.; Carlotto, S.; Rando, M.; Barchi, L.; Bolognesi, E.; Seraglia, R.; Bottaro, G.; Casarin, M.; Clever, G. H.; Armelao, L. Adaptive helicity and chiral recognition in bright europium quadruple-stranded helicates induced by host-guest interaction. *Cell Rep. Phys. Sci.* **2022**, *3* (1), No. 100692.

(16) Kim, D.; Kim, G.; Han, J.; Jung, O. S. Advances in 2D coordination networks for single-crystal-to-single-crystal applications beyond confined pores. *Bull. Korean Chem. Soc.* **2022**, *43* (8), 1019−1031.

(17) Chen, L.-J.; Yang, H.-B.; Shionoya, M. Chiral metallosupramolecular architectures. *Chem. Soc. Rev.* **2017**, *46* (9), 2555−2576.

(18) Wu, H. B.; Wang, Q. M. Construction of heterometallic cages with tripodal metalloligands. *Angew. Chem., Int. Ed.* **2009**, *48* (40), 7343−7345.

(19) Jiao, J.; Tan, C.; Li, Z.; Liu, Y.; Han, X.; Cui, Y. Design and assembly of chiral coordination cages for asymmetric sequential reactions. *J. Am. Chem. Soc.* **2018**, *140* (6), 2251−2259.

(20) Noh, T. H.; Jung, O.-S. Recent advances in various metal−organic channels for photochemistry beyond confined spaces. *Acc. Chem. Res.* **2016**, *49* (9), 1835−1843.

(21) Xue, W.; Ronson, T. K.; Lu, Z.; Nitschke, J. R. Solvent drives switching between Λ and Δ metal center stereochemistry of M_8L_6 cubic cages. *J. Am. Chem. Soc.* **2022**, *144* (14), 6136−6142.

(22) Wagner, P.; Rominger, F.; Gross, J. H.; Mastalerz, M. Solvent-controlled quadruple catenation of giant chiral [8+ 12] salicylimine cubes driven by weak hydrogen bonding. *Angew. Chem., Int. Ed.* **2023**, *62* (14), No. e202217251.

(23) Tan, C.; Chu, D.; Tang, X.; Liu, Y.; Xuan, W.; Cui, Y. Supramolecular coordination cages for asymmetric catalysis. *Chem. - Eur. J.* **2019**, *25* (3), 662−672.

(24) Balla, J.; Kiss, T.; Jameson, R. F. Copper(II)-catalyzed oxidation of catechol by molecular oxygen in aqueous solution. *Inorg. Chem.* **1992**, *31* (1), 58−62.

(25) Dey, S. K.; Mukherjee, A. Catechol oxidase and phenoxazinone synthase: Biomimetic functional models and mechanistic studies. *Coord. Chem. Rev.* **2016**, *310*, 80−115.

(26) Sekretaryova, A.; Jones, S. M.; Solomon, E. I. O_2 reduction to water by high potential multicopper oxidases: contributions of the T1 copper site potential and the local environment of the trinuclear copper cluster. *J. Am. Chem. Soc.* **2019**, *141* (28), 11304−11314.

(27) Ramadan, A.; Shaban, S.; Ibrahim, M. M.; El-Shami, F.; Al-Harbi, S. Ternary complexes containing Copper(II), L-Valinate and α, ά-bipyridyl or 1, 10-phenanthroline: Synthesis, characterization, ligand substitution and oxidase biomimetic catalytic activity studies. *J. Mol. Struct.* **2019**, *1189*, 360−376.

(28) Mouadili, A.; Zerrouki, A.; Herrag, L.; Hammouti, B.; El Kadiri, S.; Touzani, R. Catechol oxidation: activity studies using electron-rich nitrogen-based ligands. *Res. Chem. Intermed.* **2012**, *38*, 2427−2433.

(29) Shahrokhian, S.; Hamzehloei, A. Electrochemical oxidation of catechol in the presence of 2-thiouracil: application to electro-organic synthesis. *Electrochem. Commun.* **2003**, *5* (8), 706−710.

(30) Kim, D.; Lee, S.; Lee, Y. A.; Jung, O.-S. Insight into anion effects on catechol oxidation catalysis: cyclodimeric Cu(II) complexes containing 1, 3, 5-tris (nicotinoyloxy-methyl)benzene. *Transit. Met. Chem.* **2020**, *45*, 65−70.

(31) Kamau, P.; Jordan, R. Kinetic study of the oxidation of catechol by aqueous copper(II). *Inorg. Chem.* **2002**, *41* (12), 3076−3083.
(32) Dutta, S.; Bhunia, P.; Mayans, J.; Drew, M. G.; Ghosh, A. Roles of basicity and steric crowding of anionic coligands in catechol oxidase-like activity of Cu(II)−Mn(II) complexes. *Dalton Trans.* **2020**, *49* (32), 11268−11281.
(33) Kim, D.; Gwak, G.; Han, J.; Kim, D.; Jung, O.-S. Structural properties of $[Cu(II)_3L_6]$ cages: bridged polyatomic anion effects on unprecedented efficiency of heterogeneous catechol oxidation. *Dalton Trans.* **2022**, *51* (15), 5810−5817.
(34) Yang, L.; Lee, Y.-A.; Jung, O.-S. Unprecedented coordination solvate effects of bimetallic copper(II) cages on catechol oxidation catalysis. *Inorg. Chem. Commun.* **2019**, *104*, 48−53.
(35) Budisa, N.; Schneider, T. Expanding the DOPA universe with genetically encoded, mussel-inspired bioadhesives for material Sciences and medicine. *ChemBioChem.* **2019**, *20* (17), 2163−2190.
(36) Kurian, N. K.; Bhat, S. G. Food, cosmetic and biological applications of characterized DOPA-melanin from Vibrio alginolyticus strain BTKKS3. *Appl. Biol. Chem.* **2018**, *61*, 163−171.
(37) Nicklisch, S. C.; Waite, J. H. Mini-review: The role of redox in Dopa-mediated marine adhesion. *Biofouling* **2012**, *28* (8), 865−877.
(38) Zhu, W.; Peck, Y.; Iqbal, J.; Wang, D.-A. A novel DOPA-albumin based tissue adhesive for internal medical applications. *Biomaterials* **2017**, *147*, 99−115.
(39) Chan, S. W.; Dunlop, R. A.; Rowe, A.; Double, K. L.; Rodgers, K. J. L-DOPA is incorporated into brain proteins of patients treated for Parkinson's disease, inducing toxicity in human neuroblastoma cells in vitro. *Exp. Neurol.* **2012**, *238* (1), 29−37.
(40) Ogawa, M.; Murae, M.; Gemba, R.; Irie, T.; Shimojima, M.; Saijo, M.; Noguchi, K.; Fukasawa, M. L-DOPA, a treatment for Parkinson's disease, and its enantiomer D-DOPA inhibit severe fever with thrombocytopenia syndrome virus infection in vitro. *J. Infect. Chemother.* **2022**, *28* (3), 373−376.
(41) Naveen, K.; Lee, H.; Lee, D.; Lee, J. J.; Moon, J.-M.; Shim, Y.-B.; Jung, O.-S. Chiral cyclodimeric zinc(II) complexes: Enantio-recognition via differential pulse voltammetry. *Cryst. Growth Des.* **2018**, *18* (10), 6266−6272.
(42) Kim, D.; Seo, K.-D.; Moon, D.; Shim, Y.-B.; Lee, S. H.; Jung, O.-S. Chiral Pd_6L_8 nanocube pairs: Recognition of chiral amino acids via electrochemistry. *Inorg. Chem.* **2020**, *59* (9), 5808−5812.
(43) Kim, D.; Park, J.; Kim, G.; Lee, S.; Hossain, M. M.; Jung, O.-S. Pair of $(Hg_2^{II})_3L_2$ chiral cages and successive transformation into $(Hg^{II})_3L_2$ chiral cages: Chiral DOPA recognition via chiral cages. *Inorg. Chem.* **2023**, *62* (27), 10605−10612.
(44) Kim, D.; Seo, K.-D.; Shim, Y.-B.; Lee, K.; Lee, S. H.; Lee, Y.-A.; Jung, O.-S. Pair of chiral 2D silver (I) enantiomers: chiral recognition of L-and D-histidine via differential pulse voltammetry. *Dalton Trans.* **2022**, *51* (15), 6046−6052.
(45) Kissinger, P. T.; Heineman, W. R. Cyclic voltammetry. *J. Chem. Educ.* **1983**, *60* (9), 702.
(46) Shin, J. W.; Eom, K.; Moon, D. BL2D-SMC, The supra-molecular crystallography beamline at the Pohang Light Source II. *Korea. J. Synchrotron Radiat.* **2016**, *23*, 369−373.
(47) Otwinowski, Z.; Minor, W. Processing of X-ray diffraction data collected in oscillation mode. *Meth. Enzymol.* **1997**, *276*, 307−326.
(48) Sheldrick, G. *Program for empirical absorption correction of area detector data*; SADABS, 1996.
(49) Sheldrick, G. M. Crystal structure refinement with SHELXL. *Acta Crystallogr., Sect. C: Struct. Chem.* **2015**, *71*, 3−8.
(50) Kim, D.; Han, J.; Jung, O.-S.; Lee, Y.-A. Insight into systematic formation of hexafluorosilicate during crystallization via self-assembly in a glass vessel. *RSC Adv.* **2022**, *12* (39), 25118−25122.
(51) Ryu, M.; Lee, Y.-A.; Jung, O.-S. Rigid 2D networks of copper(II) complexes containing diallylbis(pyridin-3-yl)silane: Insight into anion and media effects on catechol oxidation catalysis. *J. Mol. Struct.* **2018**, *1152*, 321−327.
(52) Chen, L.; Liu, S.; Chang, F.; Xie, X.; Zhu, Z. A gold nanoparticles−enhanced carbon nanotubes electrochemical chiral sensor. *Electroanalysis* **2017**, *29* (4), 955−959.

https://doi.org/10.1021/acsomega.3c05659
ACS Omega 2023, 8, 39720−39729